CHAPTER 5

NUMERICAL ANALYSIS OF ORIGAMI STENT GRAFT

In Chapter 3, it is found that when the elements of the origami stent graft are connected in a longitudinal direction, there is a geometric mismatch between the elements. Therefore, the folds of the stent graft are deformed and the strain builds up during deployment. In this chapter further analysis is carried out in order to understand the strain level and overall deformation of the stent graft during deployment and to verify analytical formulation. The deformed shape of a thin cylindrical tube without any folds is also identified and is compared with the pattern of folds for the origami stent graft. Since the geometry of the stent graft is complicated, they can only be analysed numerically using the finite element method (FEM). We assume that the stent graft is made of shape memory alloy (SMA) because it is the material of which current stents and stent grafts are made. For the sake of simplicity, the material nonlinearity is not considered in this chapter, and only the geometrical nonlinearity is taken into account.

5.1 Strains within a fold

In this section, we examine how the strain within a fold varies with respect to the fold width when the stent graft is being folded. The data will be useful to make decisions regarding the groove width.

5.1.1 Origami stent FE model

The FE model of the origami stent graft is constructed as follows. The stent graft is a cylindrical tube and consists of units[3] with folds as shown in Figure 5.1(a). The diameter of the tube is 25.46 mm, which is similar to the actual size of the oesophageal and aortal stent grafts. The pattern of folds is the same one described in Chapter 3, where the angles of the unit: $\alpha_1 = \alpha_2 = 45^o$. Since the pattern of the folds is rotationally symmetric, in this section, to simplify the analysis, only a quarter of the model in the circumferential direction is created shown as a dark green colour in Figure 5.1(a). There are two square units and the size of the each unit is 10 mm x 10 mm.

In order to produce the designed grooves in the model, 3D solid elements are used instead of shell elements because the shell element is not able to simulate the required groove shape shown in Figure 5.1(b). The model can be divided into three layers in the radial direction and their thicknesses from the outer layer are 0.04 mm, 0.01 mm and 0.04 mm. As shown in Figure 5.1(c) and (e), the grooves for the diagonal and rectangle folds are produced in the inner and outer layers of the model. The width of the diagonal groove in the inner layer is 0.442 mm. The outer layer has grooves of 0.625 mm width, and the width of the mid groove varies to 0.3125, 1.25 and 2.5 mm. In the inner layer shown in Figure 5.3(c), 6 - node solid elements with dimensions of 0.3125 mm x 0.3125 mm x 0.04 mm in size are used. 8 - node solid elements are used for the middle and outside layers shown in Figures 5.3(d) and (e). The sizes of the elements in the middle and outer layer are 0.3125 mm x 0.3125 mm x 0.01 mm and 0.3125 mm x 0.3125 mm x 0.04 mm, respectively.

The mesh of the model is generated by codes written in MATLAB (version 6). The same mesh density is used for the entire model. Therefore, the total number of the elements is quite large, which is not ideal for the FEM model. A minimum number for the elements has been identified in the next section, which gives reduced element

[3] In the other chapters, a unit is termed as an element. To avoid confusion with elements of the FEM, we use term unit instead in this chapter.

numbers of 7632, 7440, 7056 and 6288 for the mid groove widths of 0.3125, 0.625, 1.25 and 2.5 mm, respectively.

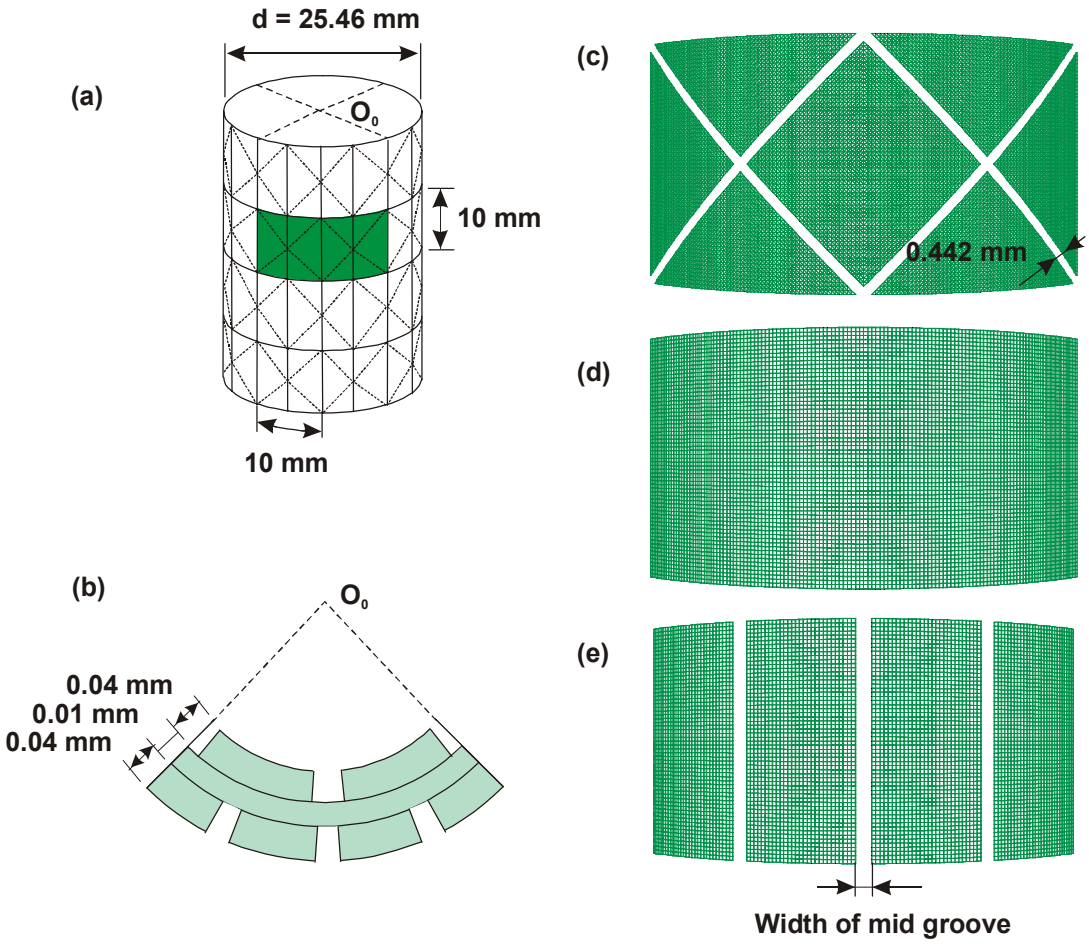

Figure 5.1 (a) Perspective view of a stent graft model; (b) cross section pair of adjustment units; (c) inner, (d) middle and (e) outer layers of the units.

The boundary conditions are shown in Figure 5.2. In a cylindrical coordinate system, both side edges of the units are fixed in the circumferential direction, and the upper edge is fixed vertically. To simulate the folding process, the 8 mm prescribed displacements are applied at the centre of the each unit pointing inwards in the radial direction, shown as red arrows in Figure 5.2(b). The use of prescribed displacements make it easy to achieve the desired deformed shape of the stent graft. Outwardly directed radial forces of 50 N are applied at the top and bottom of the units as shown by blue arrows in Figure 5.2(b). These simulate the forces during folding of the stent graft. When it is folded, the centre of the unit is pushed inwards and both edges at the top and bottom are pushed outwards.

An ABAQUS stabilisation algorithm has been applied to the FE analysis of the buckling model. It is assumed that the stent graft is made of SMA with the Young's modulus E = 60 GPa, and Poisson's ratio ν = 0.3.

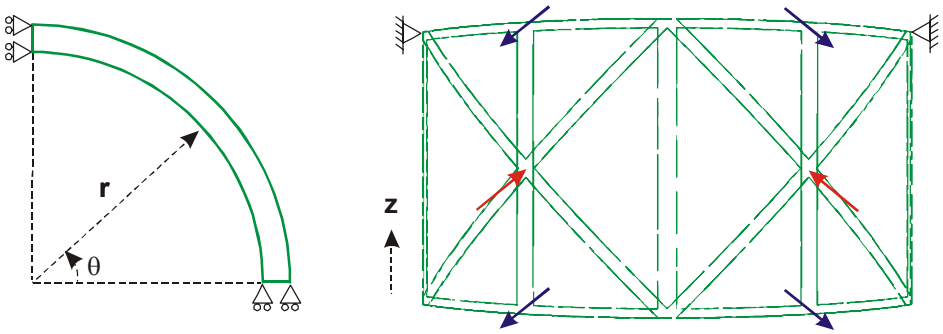

Figure 5.2 Boundary condition. (a) End and (b) perspective views

5.1.2 Performance of the element

Before carrying out FE analysis of the model, the suitability of the solid element for the stent model is examined. In reality the thickness of the stent graft is very small in comparison with its diameter and length. This results in a restriction on the sizes of the employed solid element. For numerical stability the ratio among the side length of the solid element cannot be too large or small. Hence, to achieve the same mesh density over the whole model, a huge number of elements have to be used. As a consequence, the computational cost will be very high. To reduce the computational cost, a higher ratio should be used for the stent model. Therefore, the minimum number of elements needed to simulate a groove must be found.

A simple model of a beam with a groove at the centre is created, and shown in Figure 5.3. The length and width of the beam are 33.6 mm and 2.40 mm. The depth of the groove is 0.096 mm but it is halved at the centre of the beam. The groove width is 1.2 mm.

The beam is modelled using 8 - node solid elements. The numbers of elements at the groove in the x, y and z directions are denoted as n_x, n_y and n_z, respectively. Because the dimensions of the groove are predetermined, higher numbers of elements lead to smaller elements. For example, when $n_x = 2$, $n_y = 8$ and $n_z = 4$, the side lengths of an element in the x, y and z directions are 0.6 mm, 0.3 mm and 0.012 mm with the corresponding ratio of 50:25:1. Table 5.1 summarises the various numbers examined.

The beam is simply supported at both ends and the loads are applied through prescribed displacements, -10 mm, in the z direction at the positions of 9.6 mm from each end.

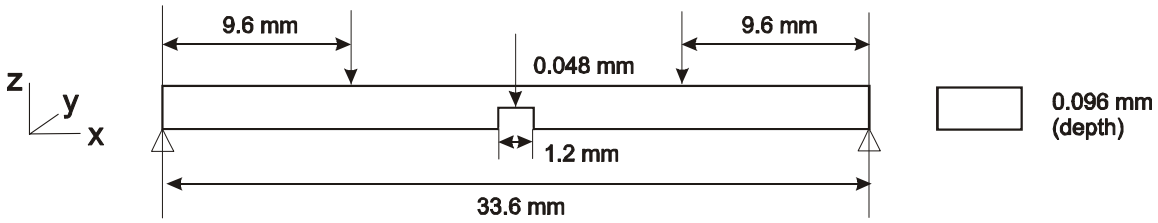

Figure 5.3 (a) A beam with a groove at the centre.

Table 5.1 The number and size of the elements of the models when groove width is 1.2 mm.

n_x	n_y	n_z	**x** x **y** x **z** (mm)
2	8	4	**0.6** x 0.3 x 0.012
4	8	**2**	0.3 x 0.3 x **0.024**
4	8	**4**	0.3 x 0.3 x **0.012**
4	8	**8**	0.3 x 0.3 x **0.006**
8	8	4	**0.15** x 0.3 x 0.012
10	8	4	**0.1** x 0.3 x 0.012

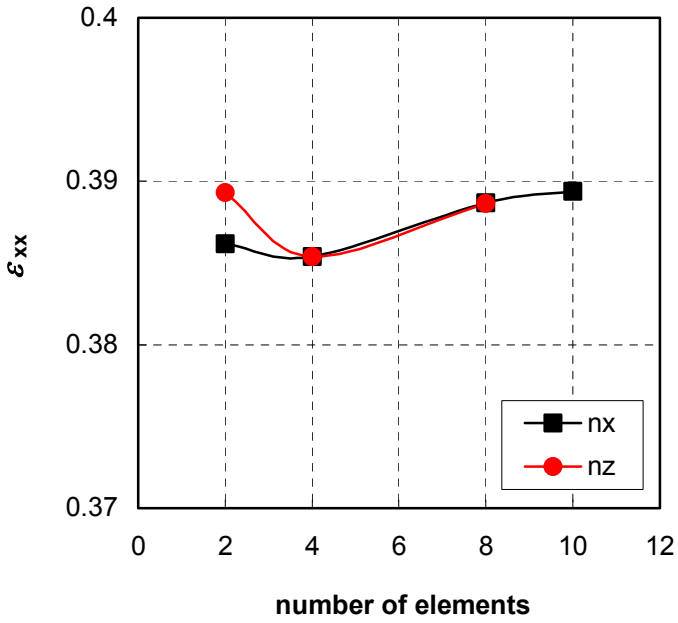

Figure 5.4 Number of elements of n_x or n_z vs. strain at the groove.

Figure 5.4 shows the results of strains ε_{xx} at the centre of the beam versus n_x or n_z. The maximum differences of ε_{xx} between the two analyses are 0.0040, corresponding to an error of 1%. It can be seen that the results are not sensitive with the change of the ratios between element side lengths. Therefore, it is possible to use fewer elements in the numerical simulation.

5.1.3 Results

Figure 5.4(a) shows the deformed shape of a pair of adjacent units when the stent graft is folded. Both valley and hill creases are visible. The position of the nodes between C_1 and C_2 is denoted as n_A (1, 2,⋯and 32), see Figure 5.4(b). The diagram of the circumferential strain $\varepsilon_{\theta\theta}$ is given in Figure 5.5. The strain becomes smaller as the width of the groove becomes wider. It is noted that the values of the strain become almost identical when the widths of the groove are 1.2 mm and 2.4 mm. Thus increasing groove width does not necessarily reduce strain.

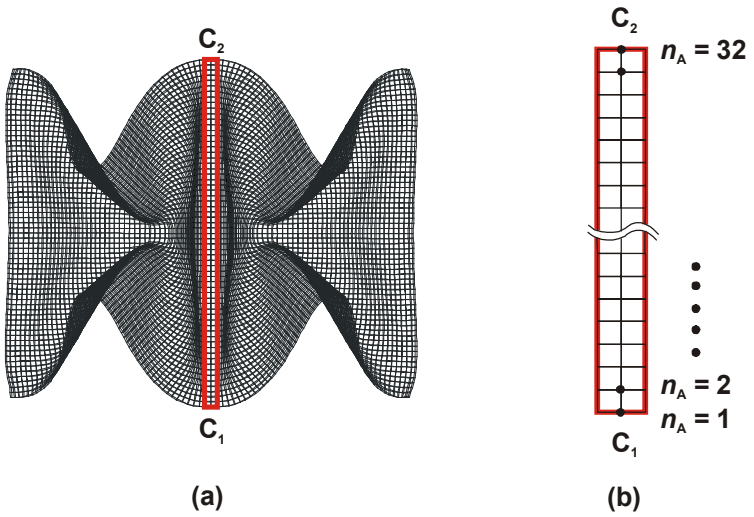

Figure 5.4 (a) Middle layer of the model in the folded configuration and (b) the position n_A of the centre fold between C_1 - C_2.

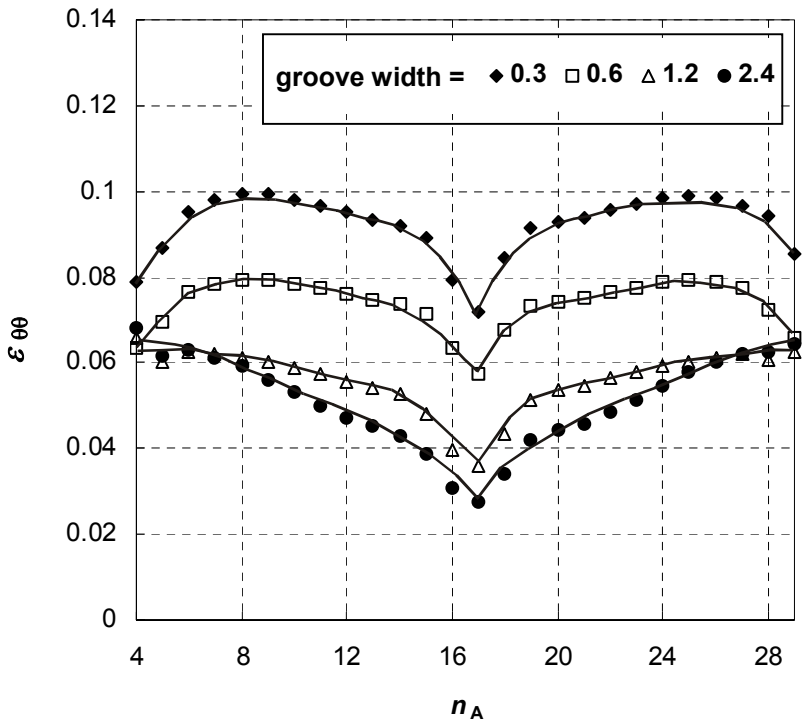

Figure 5.5 Circumferential strain $\varepsilon_{\theta\theta}$ vs. positions of nods n_A for different groove width.

5.2 Deformed shape of a thin cylindrical tube

In this section the deformed shape of a thin cylindrical tube without any folds is identified. The result will be compared with the pattern of folds for the origami stent graft.

Figure 5.6 shows a quarter section of the 0.01mm thick cylindrical tube model. The diameter of the tube is 25.46 mm. The boundary conditions in the cylindrical coordinate system are the same as those applied to the model presented previously. In the numerical analysis, a set of forces and displacement are applied, which simulate the folding process of the stent graft, see Figure 5.6(b). All of these forces are in radial directions. The prescribed displacements are applied at the centre of the each unit. These are 12 mm pointing inwards in the radial direction, and are shown by red arrows. The loads of 50 N outward the radial direction are given at the top and bottom of the unit, and are shown by blue arrows. The material is same as that used in the last section.

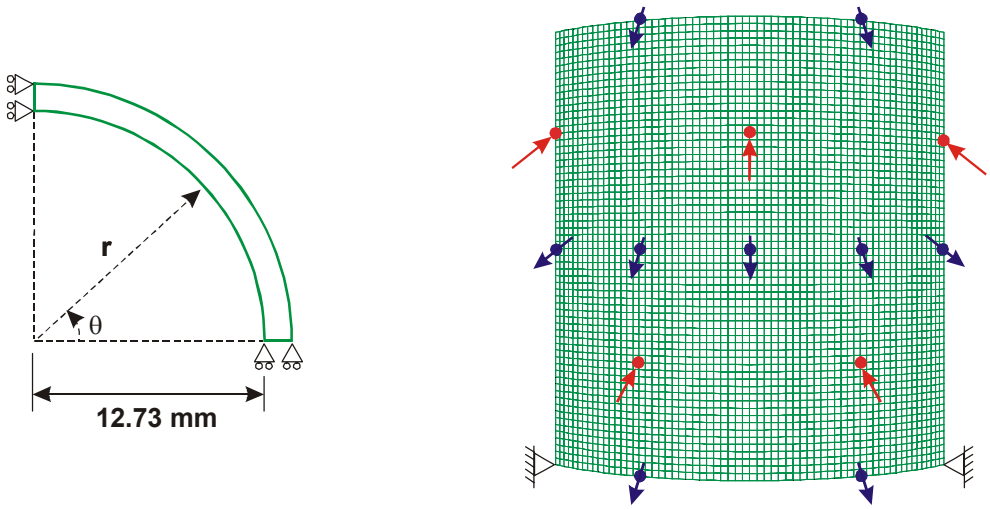

Figure 5.6 Boundary conditions of thin-tube model under a certain condition.
(a) End and (b) perspective views of the model.
Displacement of 12 mm into and 50 N outward the radial direction.

Figure 5.7(a) shows the deformed cylindrical tube. Hill and valley creases appeared on the surface of the tube and are represented by red and blue lines. The patterns of the folds are redrawn in a two-dimensional representation of the cylindrical surface as shown in Figure 5.7(b). It is found that the pattern of folds is the same as that of the foldable cylindrical tube described in Chapter 3. Therefore, if a cylindrical tube has prefabricated additional grooves for these natural folds, it will assist the folding process. Alternatively, this deformed shape can also be achieved if they are applied using mechanical methods, e.g., the application of a press. By this latter method, the cylindrical tube could be folded into the desired pattern without using folds.

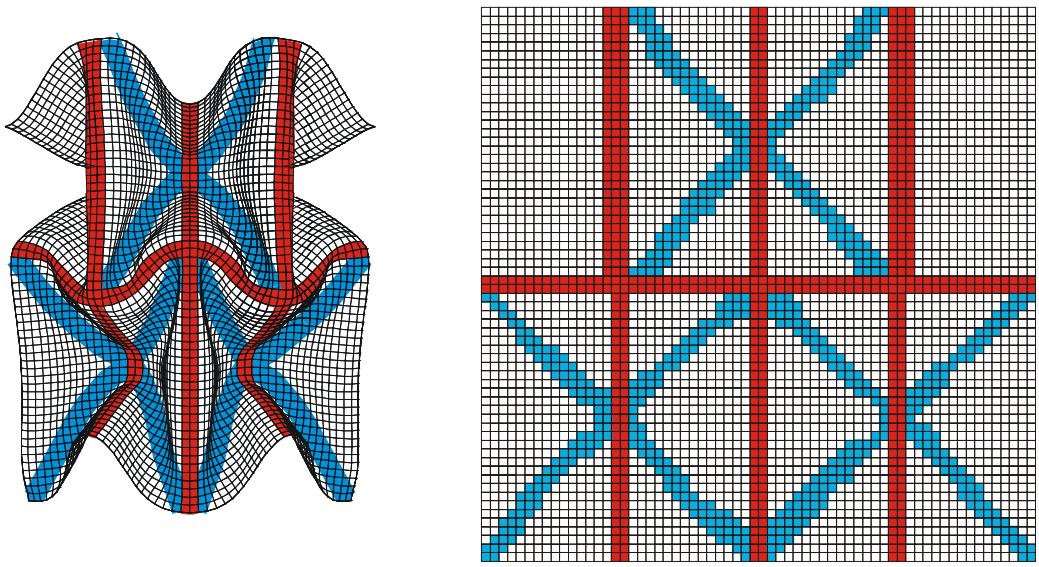

Figure 5.7 (a) Folding shape in 3D and (b) folding pattern in 2D.

5.3 Deformation of the fold

As described in Chapter 3, there is geometric mismatch among units. A simple geometric evaluation was accomplished. Now we employ the FEM to gain a more precise description of the length condition of folds. The results will be compared with the results calculated geometrically in Chapter 3.

The stent graft model is shown in Figure 5.8(a). The distance of the fold between nodes E_2A_1 and F_2B_1 is denoted l_a and calculated as follows. Firstly, the nodes E_2A_1 and F_2B_1 are defined in the cylindrical coordinates system as (R_{E2A1} , δ_{E2A1} , Z_{E2A1}) and (R_{F2B1} , δ_{F2B1} , Z_{F2B1}), respectively. Therefore, l_a is calculated by

$$l_a = \left[\left(R_{E2A1} \cos \delta_{E2A1} - R_{F2B1} \cos \delta_{F2B1} \right)^2 + \left(R_{E2A1} \sin \delta_{E2A1} - R_{F2B1} \sin \delta_{F2B1} \right)^2 + \left(Z_{E2A1} - Z_{F2B1} \right)^2 \right]^{\frac{1}{2}} \quad (5.1)$$

All variables in Equation (5.1) can be determined from the FE analysis. The FE model is similar to that in Section 5.1 except that the model has two rows of units instead of one (Figure 5.8). The widths of the grooves in the inside and outside layers are 0.442 mm and 0.625 mm, respectively. The total number of elements is 14752.

In the cylindrical coordinate system, the sides of the model are fixed in the circumferential direction and the upper edge is fixed vertically. The prescribed displacements of 12 mm inwards in the radial direction on the unfolded model are applied at the centre of the each unit, as shown in Figure 5.8(b), and the loads of 50 N outwards in the radial direction are applied at the top and bottom of the unit. The material used is, again, has the same properties as those previously used.

During the analysis, the inner radius R_i, which is the distance between node K and O_0 at the central axis, is also calculated.

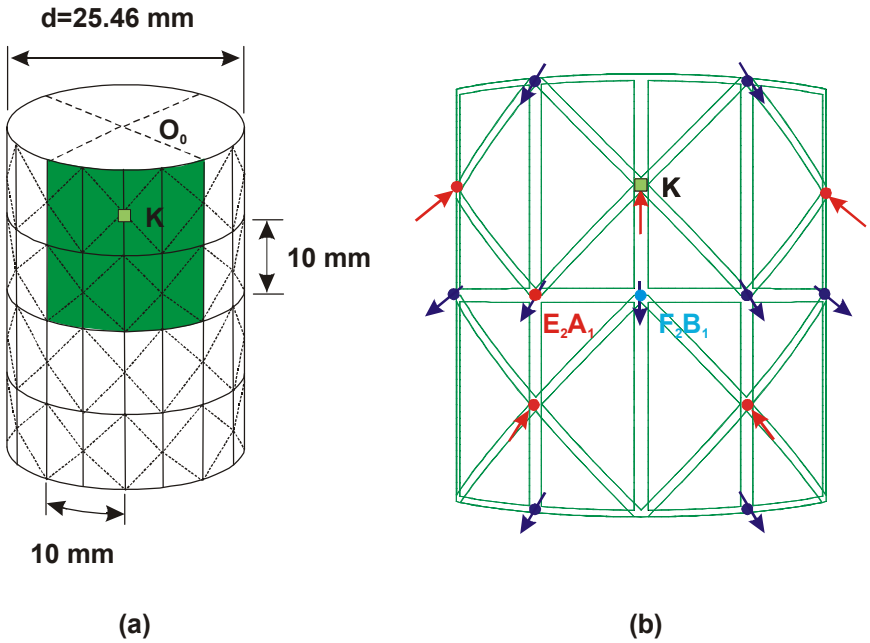

Figure 5.8 (a) The FE model with two rows of a total four units. (b) Loadings.

Figure 5.9 shows a series of images during the folding process starting with Figure 5.9(a) in its unfolded configuration. Valley and hill creases become visible from Figure 5.9(c) onwards. In Figure 5.9(h) the model is folded compactly where the control displacement of -12 mm at node K is achieved (i.e. -12 mm in the radial direction from the position of the node in the unfolded model). The inner radius R_i becomes 0.692 mm.

R_i is taken as the controlling parameter for the folding process. Figure 5.10 shows the radii of nodes E_2A_1 and F_2B_1 versus R_i. For comparison, $(R_{o1}+R_{o2})/2$ the radius of the nodes E_2A_1 and F_2B_1 calculated analytically in Chapter 3 is also shown. It is found that the results are almost identical. Figure 5.11 shows the difference between $Z_{E2A1} - Z_{F2B1}$ versus R_i. The FEM result is smaller than those achieved by the geometrical analysis. It is probably because the fold between the nodes E_2A_1 and F_2B_1 is curved during numerical analysis, while it kinks in the geometric analysis. Figure 5.12 shows a plot of l_a / l_o versus R_i. These results are clearly different from the result calculated by the

geometric analysis. The difference is around 18% when the tube is fully folded, to 1% when it is expanded.

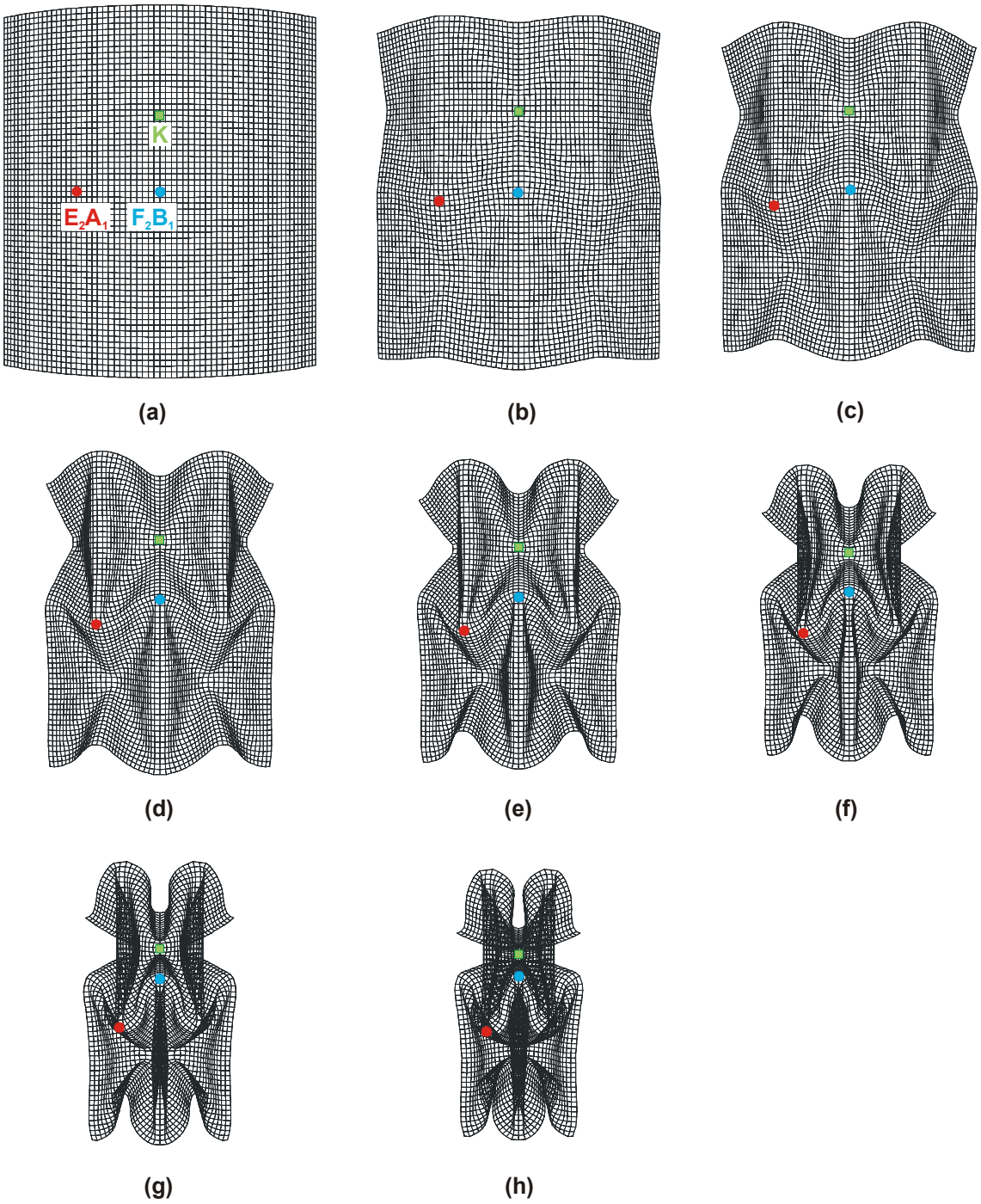

Figure 5.9 Series of photos showing the folding process. The controlling radius R_i = (a) 12.69, (b) 11.92, (c) 9.807, (d) 8.452, (e) 7.102, (f) 5.752, (g) 4.042 and (h) 0.692 mm.

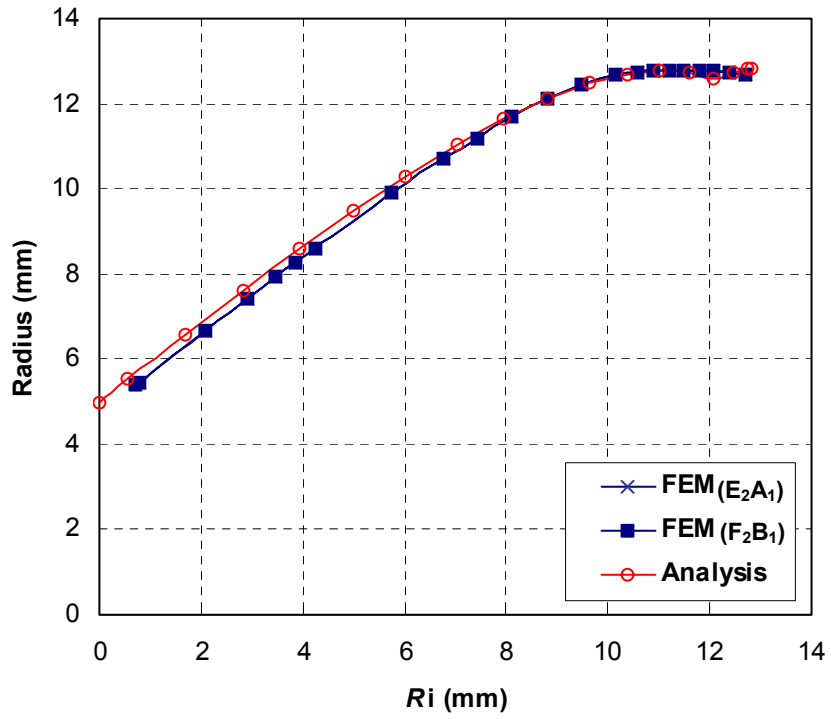

Figure 5.10 Radii vs. R_i.

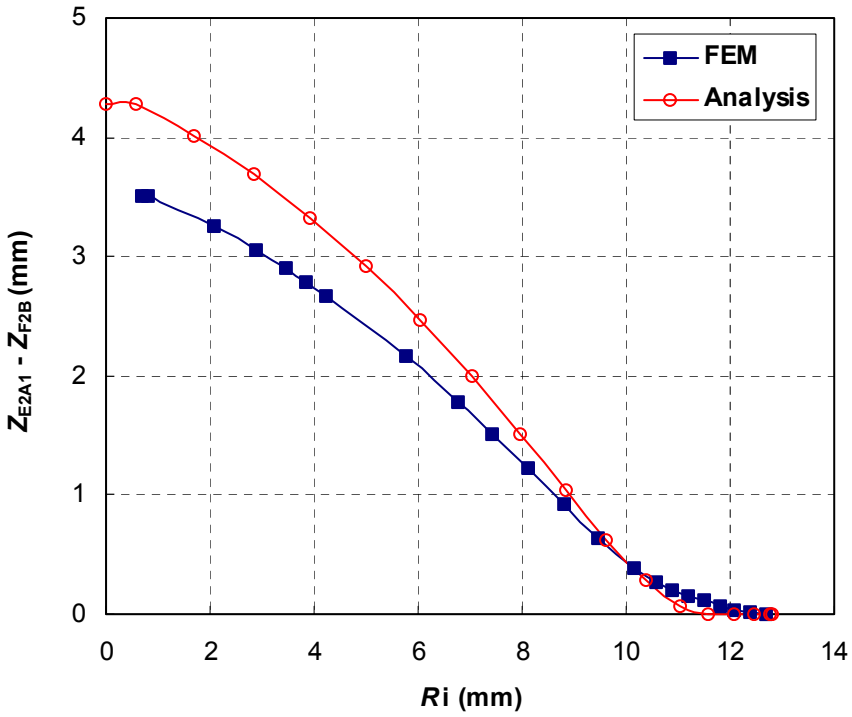

Figure 5.11 Z_{E2A1} - Z_{F2B} vs. R_i.

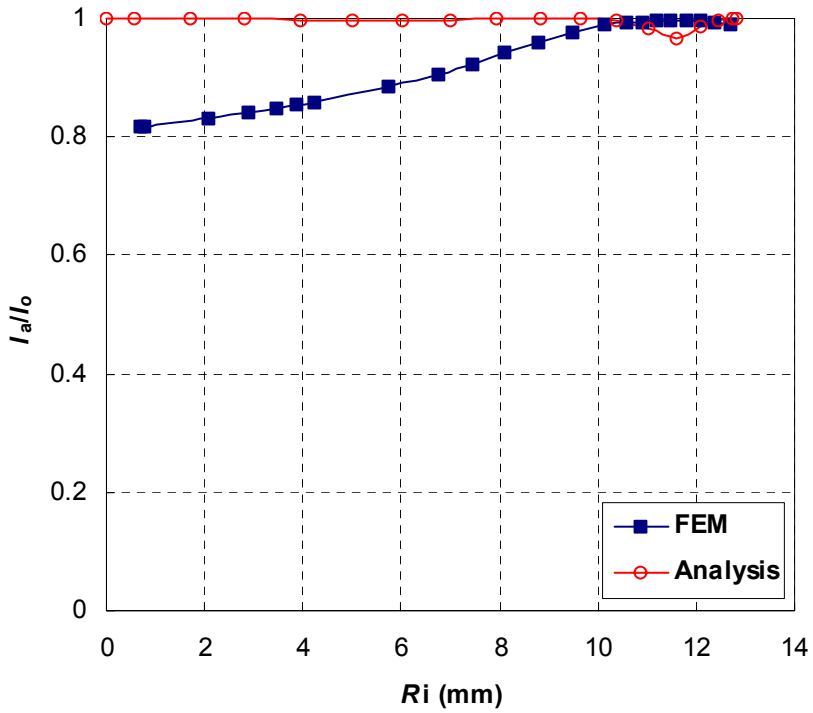

Figure 5.12 I_a/I_o **vs.** R_i.

5.4 Conclusions

In this chapter FE analysis has been carried out to understand the strain of the fold with respect to the different widths of the fold. Also, the pattern of the deformed thin cylindrical tube without any folds has been analysed. The main results are summarised as follows.

It is found that the circumferential strain becomes smaller as the width of the groove increases. However, the reduction of the strain becomes less obvious when the width is larger than 1.2 mm.

The geometry of the deformed pattern resembled the pattern of the folds that was found in the foldable cylindrical tube described in Chapter 3. The geometry of the deformed pattern resembles the pattern of the folds of the designed foldable cylindrical tube. Therefore, the stent graft can be folded into the desirable shape easily if the groove

is produced. By the press method, the cylindrical tube could be folded into the desired pattern without using folds.

FE analysis is also used to identify the accuracy of the geometric analysis in the presence of mismatch. It is found that the geometric analysis and FEM techniques strongly agree with one another with regard to deployment radius, but weakly agree in assessing overall length.